ИЗВЕСТИЯ ВЫСШИХ УЧЕБНЫХ ЗАВЕДЕНИЙ.
Т 65 (4) Серия «**ХИМИЯ И ХИМИЧЕСКАЯ ТЕХНОЛОГИЯ**» 2022

IZVESTIYA VYSSHIKH UCHEBNYKH ZAVEDENII
V 65 (4) **KHIMIYA KHIMICHESKAYA TEKHNOLOGIYA** 2022
RUSSIAN JOURNAL OF CHEMISTRY AND CHEMICAL TECHNOLOGY

DOI: 10.6060/ivkkt.20226504.6550

ВЛИЯНИЕ ЛЕГИРУЮЩИХ ЭЛЕМЕНТОВ Zn И Zr НА КОРРОЗИОННОЕ ПОВЕДЕНИЕ АМОРФНЫХ СПЛАВОВ ALCUMG (Zn) И ALCUMG (Zr) И ИХ НАНОКРИСТАЛЛИЧЕСКИХ АНАЛОГОВ

В.Л. Дякова, Й.Г. Костова, Б.Р. Цанева

Ваня Любомирова Дякова *, Йоанна Георгиева Костова

Институт металловедения, оборудования и технологий с гидроаэродинамическим центром Болгарской Академии Наук, ул. Шипченски проход, 67, 1574 София, Болгария
E-mail: v_diakova@ims.bas.bg*, joanna_hristova@abv.bg

Боряна Рангелова Цанева

Технический университет София, бул. Климента Охридски 8, София 1000, Болгария
E-mail: borianatz@tu-sofia.bg

Быстро затвердевшие ленты на основе сплава $Al_{74}Cu_{16}Mg_{10}$ были получены методом спиннингования. Для получения кристаллической структуры быстрозатвердевшие ленты отжигали в атмосфере аргона. Аморфная и нанокристаллическая структура подтверждена анализами XRD и TEM. Исследовано влияние легирующих элементов Zn и Zr на коррозионное поведение быстрозатвердевшего сплава $Al_{74}Cu_{16}Mg_{10}$ в аморфных и нанокристаллических аналогах. Проведены гравиметрические испытания на общую коррозию при 25 °C и 50 °C в среде 3,5% NaCl. При 25 °C скорость коррозии аморфных сплавов оказалась в 1,5–4 раза ниже скорости коррозии их кристаллических аналогов. Влияние трансформации аморфной структуры в нанокристаллическую на скорость коррозии при 50 °C отрицательно и наиболее существенно в Zn-содержащем сплаве. Проведены электрохимические испытания на общую и локальную коррозию в среде 3,5% NaCl и объяснен гальванический механизм локальной коррозии в сплавах. Основной причиной регистрируемой повышенной локальной коррозии кристаллических сплавов является химическая и структурная неоднородность, связанная с наличием в алюминиевой матрице активных интерметаллических фаз Al_2CuMg, Al_2 (Cu, Zn), Al_3Zr_4. Обсуждается влияние неровности поверхности, структуры слоя продуктов коррозии, отложенного на поверхность металла, и отжига для трансформации аморфной структуры на коррозионное поведение сплавов.

Ключевые слова: коррозия, аморфный, нанокристаллический, алюминий

Для цитирования:
Дякова В.Л., Костова Й.Г., Цанева Б.Р. Влияние легирующих элементов Zn и Zr на коррозионное поведение аморфных сплавов AlCuMg (Zn) и AlCuMg (Zr) и их нанокристаллических аналогов. *Изв. вузов. Химия и хим. технология*. 2022. Т. 65. Вып. 4. С. 62–70

For citation:
Dyakova V.L., Kostova Y.G., Tzaneva B.R. Effect of minority alloying elements Zn and Zr on the corrosion behavior of amorphous alloys AlCuMg(Zn) and AlCuMg(Zr) and their nanocrystalline analogues. *ChemChemTech* [*Izv. Vyssh. Uchebn. Zaved. Khim. Khim. Tekhnol.*]. 2022. V. 65. N 4. P. 62–70

EFFECT OF MINORITY ALLOYING ELEMENTS Zn AND Zr ON THE CORROSION BEHAVIOR OF AMORPHOUS ALLOYS ALCUMG(Zn) AND ALCUMG(Zr) AND THEIR NANOCRYSTALLINE ANALOGUES

V.L. Dyakova, Y.G. Kostova, B.R. Tzaneva

Vanya L. Dyakova*, Yoanna G. Kostova

Institute of Metal Science, Equipment and Technology with Hydro-and Aerodynamics Centre of Acad. A. Balevski at Bulgarian Academy of Sciences, Shipchenski Prohod st., 67, Sofia, 1574, Bulgaria
E-mail: v_diakova@ims.bas.bg*, joanna_hristova@abv.bg

Boriana R. Tzaneva

SofiaTechnical University, Kliment Ohridski Blvd., 8, Sofia, 1000, Bulgaria
E-mail: borianatz@tu-sofia.bg

Rapidly solidified ribbons based on $Al_{74}Cu_{16}Mg_{10}$ alloy were produced by Chill Block Melt Spinning (CBMS) method. In order to obtaine a crystalline structure the rapidly solidified ribbons were annealed in Ar atmosphere. The amorphous and nanocrystalline structure was confirmed by XRD and TEM analyzes. The effect of minority alloying elements Zn and Zr on the corrosion behavior of rapidly solidified $Al_{74}Cu_{16}Mg_{10}$ alloy in amorphous and nanocrystalline analogues was studied. Gravimetric tests for general corrosion at 25 °C and at 50 °C in environment of 3.5% NaCl are carried out. At 25 °C the corrosion rate of amorphous alloys was found to be 1.5 to 4 times lower than the rate of their crystalline analogues. The effect of amorphous - nanocrystalline structure transformation on the corrosion rate at 50 °C is negative and most significant in the Zn-containing alloy. Electrochemical tests for general and local corrosion in 3.5% NaCl environment were performed and the galvanic mechanism of local corrosion in alloys was explained. The main reason for the registered enhanced local corrosion in the crystalline alloys is the chemical and structural inhomogeneity due to the presence of the active intermetallic phases Al_2CuMg, $Al_2(Cu,Zn)$, Al_3Zr_4 in the aluminum matrix. The influence of the surface irregularity, of the structure of the layer of corrosion products deposited on the metal surface and of the annealing for the transformation of the amorphous structure on the corrosion behavior of the alloys are discussed.

Key words: corrosion, amorphous, nanocrystalline, aluminum

INTRODUCTION

The first evidence on the high corrosion resistance of metallic glasses from the Fe-Cr system was reported in 1974 [1]. Since then, a lot of studies have been published on the corrosion behavior of amorphous alloys based on Fe [2, 3], Zr [4, 5], Al [6, 7]. The important role of the chemical composition in the corrosion behavior of metallic glasses is well known [9], while the role of the amorphous structure is not yet well understood. There are contradictory literature data on the corrosion resistance of amorphous alloys compared to their crystalline analogues [8]. The amorphous alloys usually demonstrate high corrosion resistance which is most often explained by their structural homogeneity, lack of defects and ability to form supersaturated solid solutions with the alloying elements but it has been found that in some cases their corrosion resistance is not higher in spite of their homogeneous and defect-free microstructure [10].

It is known that in corrosion conditions the amorphous metals form two types of covering films – amorphous and a mixture of amorphous and crystalline. The structure and the type of the covering film determine the different corrosion behavior in amorphous and crystalline state. The homogeneous chemical composition and microstructure of amorphous glasses promotes the formation of amorphous oxide on the surface [11]. The dense amorphous film of uniform thickness and structure prevents the ions diffusion towards and from the metal surface, restricts the development of the corrosion process and provides good protection of the metal. The oxy-hydroxide film is a mixture of amorphous and crystalline oxides. It is uneven in thickness and coverage due to the presence of phase boundaries between amorphous and crystalline oxides and so impairs its protective ability [12, 13].

The aim of our work is to study the corrosion behavior of alloys of the Al-Cu-Mg system alloyed

with small amounts of Zn and Zr in amorphous and nanocrystalline state and to obtain data on their corrosion rate in 3.5% NaCl at 25 and 50 °C, as well as on their electrochemical corrosion performance.

EXPERIMENTAL PART

Tested materials

It is known that metallic glasses are most easily obtained from alloys with eutectic composition [14]. We chose $Al_{74}Cu_{16}Mg_{10}$ as a base alloy in our work, the alloy being close to the composition of the triple eutectics, point E5 from the phase diagram Al-Cu-Mg [15]. One at.% Zn and 0.3 at.% Zr were added to the base alloy. Rapidly solidified alloys were obtained by Chill Block Melt Spinning (CBMS) method in the form of ribbons 1.7 to 7 mm wide and 42 to 120 μm thick. The synthesis of Al-Cu-Mg-Zn and Al-Cu-Mg-Zr alloys and the process of obtaining the ribbons are described in detail in our previous publications [16,17]. In order to transform the structure from amorphous to nanocrystalline part of the ribbons were annealed at 300 °C for 1.5 h in argon environment in electric arc furnace. The tested rapidly solidified amorphous ribbons are designated as follows:

$Al_{74}Cu_{16}Mg_{10}$, or (3r), is the initial (base) alloy;

$(Al_{74}Cu_{16}Mg_{10})_{99}Zn$, or (3r-1%Zn), is the alloy with 1 at. % Zn;

$Al_{74}Cu_{16}Mg_{10})_{99,7}Zr_{0,3}$, or (3r-0.3at.%Zr), is alloy with 0.3 at. % Zr.

The index "a" means that the ribbons are annealed. Later in our work the rapidly solidified amorphous ribbons (r) will be called "amorphous alloys" and the annealed ribbons (a) will be called "nanocrystalline alloys".

The amorphousness of all alloys was studied and confirmed in our previous work [18] by X-ray diffraction (XRD), transmission electron microscopy (TEM) and differential scanning calorimetry (DSC). After annealing the alloys were analyzed by XRD again. The results from of the XRD analysis are shown in Fig. 1 and Table 1. The data obtained for phase content in amorphous and crystalline state are shown in Table 1 also.

The eutectic base alloy $Al_{74}Cu_{16}Mg_{10}$ is 98% amorphous. It was found that the addition of only 0.3 at.% zirconium to the base alloy is sufficient to achieve a 100% amorphous state in $(Al_{74}Cu_{16}Mg_{10})_{99.7}Zr_{0.3}$ under the same conditions of rapid solidification. And contrariwise, the addition of 1 at.%Zn reduces the 98% amorphous part of the base alloy to 71% in $(Al_{74}Cu_{16}Mg_{10})_{99}Zn$. Previous studies with higher amounts of Zn have shown that with the increase of Zn amount to 2 and 3% the amorphous part of the ribbons decreases to 49% and 45%, respectively. The results were explained in terms of free volume model (FVM) [19].

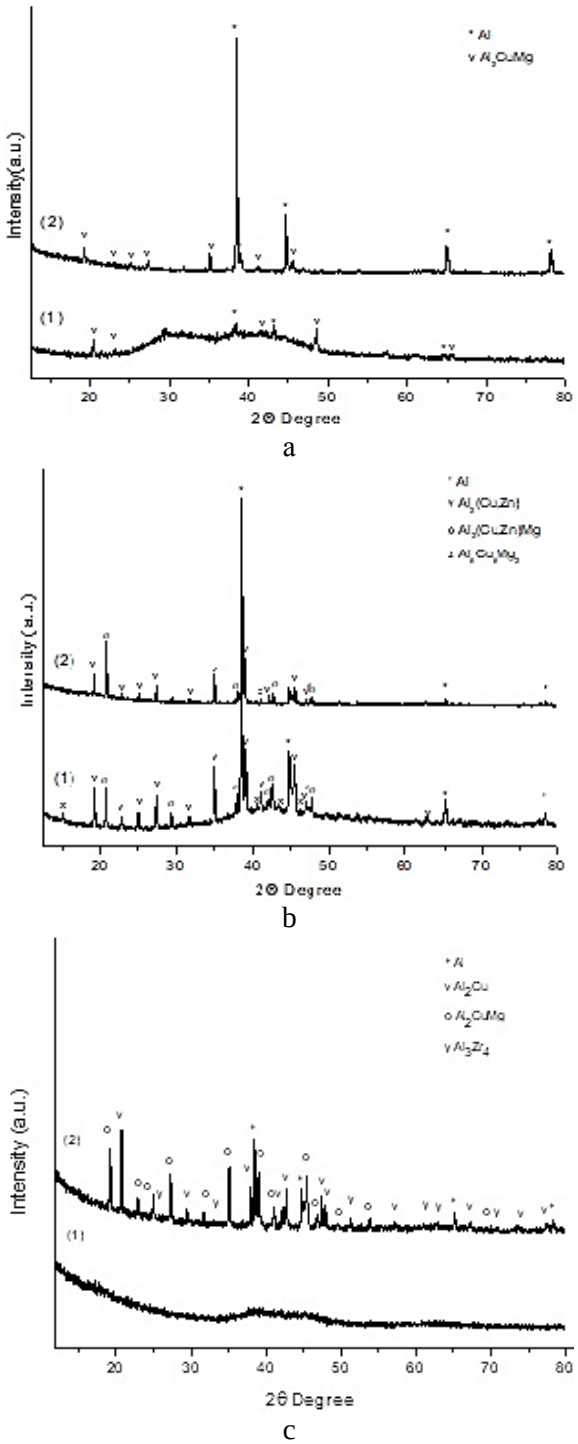

Fig. 1. XRD diagrams of amorphous (1) and nanocrystalline (2) alloys: a) AlCuMg. Amorphous base alloy 3r (1) and nanocrystalline alloy 3r-a (2); b) AlCuMg(Zn). Amorphous alloy 3r-1at.%Zn (1) and nanocrystalline alloy 3r-1at.%Zn-a (2); c) AlCuMg(Zr). Amorphous alloy 3r-0.3at.%Zr (1) and nanocrystalline alloy 3r-0.3at.%Zr-a (2)

Рис. 1. XRD диаграммы аморфных (1) и нанокристаллических (2) сплавов: a) AlCuMg. Аморфный основной сплав 3r (1) и нанокристаллический сплав 3r-a (2); b) AlCuMg(Zn). Аморфный сплав 3r-1ат.%Zn (1) и нанокристаллический сплав 3r-1ат.%Zn-a (2); c) AlCuMg(Zr). Аморфный сплав 3r-0,3ат.%Zr (1) и нанокристаллический сплав 3r-0,3ат.%Zr-a (2)

Table 1

Structural characteristics of $Al_{74}Cu_{16}Mg_{10}$, $(Al_{74}Cu_{16}Mg_{10})_{99}Zn$ and $(Al_{74}Cu_{16}Mg_{10})_{99}Zr$ amorphous and nanocrystalline alloys

Таблица 1. **Структурные характеристики аморфных и нанокристаллических сплавов $Al_{74}Cu_{16}Mg_{10}$, $(Al_{74}Cu_{16}Mg_{10})_{99}Zn$ и $(Al_{74}Cu_{16}Mg_{10})_{99}Zr$**

Designations of alloys	Amorphous part, [%]	Types of crystalline phases
$Al_{74}Cu_{16}Mg_{10}$ (3r)	98	Al; Al_2CuMg
$Al_{74}Cu_{16}Mg_{10}$-a (3ra)	-	Al; Al_2CuMg
$(Al_{74}Cu_{16}Mg_{10})_{99}Zn$ (3r-2%Zn)	71	Al; Al_2 (Cu,Zn); Al_2(Cu,Zn)Mg
$(Al_{74}Cu_{16}Mg_{10})_{99}Zn$-a (3r-2%Zn-a)	-	Al; (Cu,Zn) Al_2; Al_2(Cu,Zn)Mg
$(Al_{74}Cu_{16}Mg_{10})_{99}Zr$ (3r-1%Zr)	100	-
$(Al_{74}Cu_{16}Mg_{10})_{99}Zr$-a (3r-1%Zr-a)	-	Al; Al_2CuMg; $CuAl_2$; Al_3Zr_4

Corrosion test methods

Gravimetric corrosion test

The gravimetric corrosion method was chosen based on our previous experience of corrosion studies of aluminum alloys. The tests were carried out by continuous immersion of specimens for 360 h in medium of 3.5% NaCl at (25±1) °C and **(**50±1) °C in a thermostat. Five specimens from each studied alloy with length of about 3 cm were tested. After the test completion the corrosion products were removed using diluted HNO_3. The specimens were weighed prior to and after the test with an accuracy of 10^{-5} g.

The mass loss index Δm was calculated as $\Delta m = m_0 - m_1$, [g], where m_0 was the mass of the specimen before the testing, and m_1 was the mass after completing the test and removing the corrosion products. The corrosion rate K was calculated as $K = \frac{\Delta m}{S.t}$ [g/m^{2}h], where S [m^2] is the surface area of the specimen, and t [h] is the test duration [20].

Electrochemical corrosion tests

Electrochemical corrosion test were carried out in order to confirm the results of gravimetric tests and the galvanic mechanism of the corrosion process in $Al_{74}Cu_{16}Mg_{10}$, $(Al_{74}Cu_{16}Mg_{10})_{99}Zn$ and $(Al_{74}Cu_{16}Mg_{10})_{99.7}Zr_{0.3}$ alloys in amorphous and nanocrystalline state.

Open circuit potential measurements and potentiodynamic cyclic method were used to determine the resistance of the studied ribbons to general and local corrosion. Test specimens of 0.5 cm^2 surface area were degreased in alcohol, threated in diluted HNO_3, and immersed in a solution of 3.5% NaCl at temperature of 25 °C. A tri-electrode cell with a working electrode from the studied amorphous alloys, a platinum counter electrode and a silver chloride reference electrode (Ag/AgCl) was used. All potentials in this work are reported relative to the silver chloride electrode. The electrochemical tests were performed with Autolab galvanostat-potentiostat model PGSTAT 204 and computer software NOVA 2.1.

The specimens were kept more than10 min in 3.5% NaCl to stabilize the open circuit potential (OCP). Before starting the potentiodynamic test the surface were cathodically polarized for 60 s at -0.5V vs OCP to remove the natural passive layer. The cyclic potentiodynamic studies were carried out at a scan rate of 1 mV/s in anodic direction from initial potential of -0.5V vs OCP until exceeding the threshold anodic current density with more than 1 mA/cm^2, after which the potential scan was reversed in cathode direction to the cross-point of the forward and the backward branches of the polarization curve. For each ribbon, at least 5 tests were performed to verify the reproducibility of the results. The results of the polarization tests of AlCuMg(Zn) and AlCuMg(Zr) ribbons were compared with those obtained for pure Al (99.999%) [21].

RESULTS

Gravimetric tests

The results of the gravimetric tests for the corrosion rate K are presented in Table 2 and Fig. 2. Based on the averaged values of K at the two test temperatures, the ratios A, B, C, and D are calculated. They give information about the effect of annealing and the test temperature on the corrosion rate as follows: The ratios $A = Ka_{25}/Kr_{25}$ and $B = Ka_{50}/Kr_{50}$ show the change of the corrosion rate of each alloy after the amorphous-crystalline transformation due to annealing, at the corrosion environment temperature of 25 °C and 50 °C, respectively. Analogically the ratios $C = Kr_{50}/Kr_{25}$ and $D = Ka_{50}/Ka_{25}$ indicate the influence of the test temperature on the corrosion rate in both states – amorphous and nanocrystalline.

At 25 °C (Fig. 2) the amorphous base alloy $Al_{74}Cu_{16}Mg_{10}$ has the lowest corrosion rate Kr_{25}. The corrosion rates Kr_{25} of Zn- and Zr-containing amorphous alloys $(Al_{74}Cu_{16}Mg_{10})_{99}Zn$ and $(Al_{74}Cu_{16}Mg_{10})_{99.7}Zr_{0.3}$ are respectively about 2 and 3 times higher compared to the base alloy. Nevertheless, the corrosion rates of all three amorphous alloys remain comparatively low and do not exceed 0.02 g/m^{2}h.

At 50 °C the lowest corrosion rate Kr_{50} is obtained for the Zn-containing alloy $(Al_{74}Cu_{16}Mg_{10})_{99}Zn$ where the influence of test temperature on the corrosion rate is negligible and C = 1. The highest Kr_{50} is exhibited for the Zr-containing alloy $(Al_{74}Cu_{16}Mg_{10})_{99}Zr$.

Table 2

Corrosion rate of the test specimens after 360 h in environment of 3.5% NaCl

***Таблица 2*. Скорость коррозии испытуемых образцов через 360 ч в среде 3,5% NaCl**

Designation of the alloy	Corrosion rate K [g/m^{2}h]					
	K_{25} T = 25 °C	A Ka_{25}/Kr_{25}	K_{50} T = 50 °C	B Ka_{50}/Kr_{50}	C Kr_{50}/Kr_{25}	D Ka_{50}/Ka_{25}
$Al_{74}Cu_{16}Mg_{10}$ (3r)	0.0063	4,4	0.0352	0,7	5.6	0,86
$Al_{74}Cu_{16}Mg_{10}$-a (3r-a)	0.0280		0.0242			
$(Al_{74}Cu_{16}Mg_{10})_{99}Zn_1$ (3r-1at.%Zn)	0.0133	2,8	0.0135	-	1.01	-
$(Al_{74}Cu_{16}Mg_{10})_{99}Zn$ –a (3r-1at.%Zn-a)	0.0370		decomposed			
$(Al_{74}Cu_{16}Mg_{10})_{99.7}Zr_{0.3}$ (3r-0.3at.%Zr)	0.0177	1,7	0.0792	1.05	4.5	2.73
$(Al_{74}Cu_{16}Mg_{10})_{99}Zr$ –a (3r-0.3at.%Zr-a)	0.0305		0.0833		-	

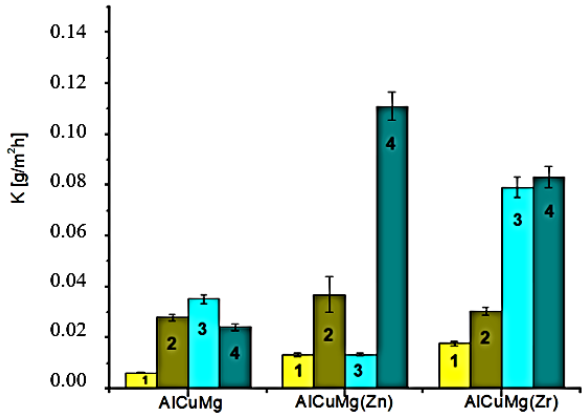

Fig. 2. Corrosion rate K in 3.5%NaCl at 25 °C (1 and 2) and 50 °C (3 and 4)

Рис. 2. Скорость коррозии K в 3,5% NaCl при 25 °C (1 и 2) и 50 °C (3 и 4)

The nanocrystalline alloys display a significantly higher corrosion rate at 25 °C compared to their amorphous analogues. The highest Ka_{25} = 0.037g/m^{2}h is obtained for the nanocrystalline alloy $(Al_{74}Cu_{16}Mg_{10})_{99}Zn$–a. It should be noted that the crystallization has the most negative effect on the base alloy $Al_{74}Cu_{16}Mg_{10}$, for which the ratio A has the highest value.

At 50 °C the effect of crystallization (the presence of crystalline phase) is considerably weaker for the base alloy $Al_{74}Cu_{16}Mg_{10}$ and the Zr-containing alloy $(Al_{74}Cu_{16}Mg_{10})_{99}Zr$. The corrosion rates in both amorphous and nanocrystalline state for these alloys are almost identical, their ratio B being close to 1. The fastest and most destructive corrosion is observed in the Zn-containing nanocrystalline alloy $(Al_{74}Cu_{16}Mg_{10})_{99}Zn$-a.

Electrochemical corrosion tests

The corrosion behavior of the alloys is studied without applying any external polarization. Fig. 3 displays the values of open circuit potentials (OCP) of amorphous (thick symbols) and nanocrystalline (hollow symbols) alloys $Al_{74}Cu_{16}Mg_{10}$, $(Al_{74}Cu_{16}Mg_{10})_{99}Zn$ and $(Al_{74}Cu_{16}Mg_{10})_{99.7}Zr_{0.3}$.

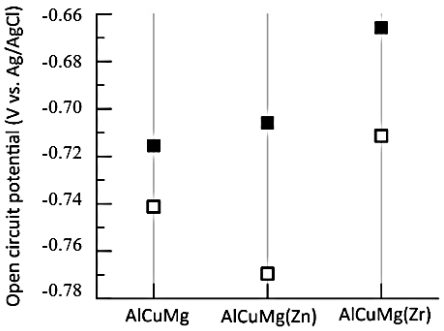

Fig. 3. OCP of amorphous (thick symbols) and nanocrystalline (hollow symbols) alloys $Al_{74}Cu_{16}Mg_{10}$, $(Al_{74}Cu_{16}Mg_{10})_{99}Zn$ and $(Al_{74}Cu_{16}Mg_{10})_{99.7}Zr_{0.3}$

Рис. 3. ПРЦ аморфных (жирные символы) и нанокристаллических (полые символы) сплавов $Al_{74}Cu_{16}Mg_{10}$, $(Al_{74}Cu_{16}Mg_{10})_{99}Zn$ и $(Al_{74}Cu_{16}Mg_{10})_{99,7}Zr_{0,3}$

The addition of small amounts of Zn and Zr to the base alloy $Al_{74}Cu_{16}Mg_{10}$ shifts the OCP of amorphous alloys in positive direction (Fig. 3). This effect is most noticeable in the Zr-containing alloy. Usually, such positive potential shift is indicative of improved corrosion resistance as a result of either inclusion of a nobler metal, or formation of passive protective layers. Since the potentials of both zinc and zirconium are strongly negative, a positive shift of OCP by these elements could be more likely associated with an improvement in the protective properties of the passive layers. In some specific cases, however, it is possible that the potential shift results from development of local forms of corrosion, in which the anode section works more intensely, with lower anode polarization.

The transformation of amorphous into nanocrystalline structure provoked by the annealing leads to destabilization of corrosion behavior of all studied alloys, which is expressed in a negative shift of the values of OCP. The negative effect of the process is most pronounced in the Zn-containing nanocrystalline alloy $(Al_{74}Cu_{16}Mg_{10})_{99}Zn$-a.

Fig. 4 displays the polarization dependencies of alloys $Al_{74}Cu_{16}Mg_{10}$, $(Al_{74}Cu_{16}Mg_{10})_{99}Zn$ and $(Al_{74}Cu_{16}Mg_{10})_{99.7}Zr_{0.3}$ in both states. The determined values of corrosion current density (i_{corr}), corrosion potential (E_{corr}), and protection potential (E_p) are shown in Fig. 5.

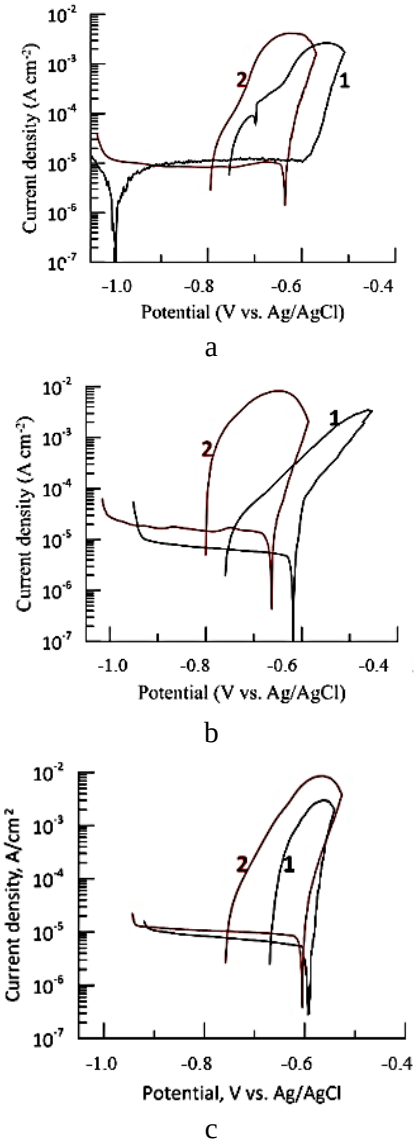

Fig. 4. OCP of amorphous (thick symbols) and nanocrystalline (hollow symbols) alloys $Al_{74}Cu_{16}Mg_{10}$, $(Al_{74}Cu_{16}Mg_{10})_{99}Zn$ and $(Al_{74}Cu_{16}Mg_{10})_{99.7}Zr_{0.3}$

Рис. 4. Поляризационные зависимости аморфных (1) и нанокристаллических (2) сплавов $Al_{74}Cu_{16}Mg_{10}$, $(Al_{74}Cu_{16}Mg_{10})_{99}Zn$ и $(Al_{74}Cu_{16}Mg_{10})_{99}Zr$. a. $Al_{74}Cu_{16}Mg_{10}$; b. $(Al_{74}Cu_{16}Mg_{10})_{99}Zn$; c. $(Al_{74}Cu_{16}Mg_{10})_{99}Zr$

The polarization dependencies reveal a broad cathodic area with a low diffusion current of the oxygen reaction. Upon reaching the corrosion potential, the anode current density increases sharply, which is indicative of intensive dissolution of the studied alloys. When the current density exceeds 1 mA/cm^2 and the polarization is reversed in cathode direction, hysteresis is observed on all dependences. The higher values of current density in reverse potential scanning are indicative of development of pitting corrosion. Upon reaching the protection potential E_p, the current density decreases sharply again. This course of the polarization dependences shows that the corrosion process in the studied alloys begins with development of pitting corrosion. The initiation and development of pitting begins at the chemical heterogeneous points or irregularity on the surfaces of the ribbons.

The effect of the Zn or Zr presence in amorphous (thick symbols) and nanocrystalline (hollow symbols) alloys AlCuMg on the corrosion current density and pitting formation potential is shown in Fig. 5. The values of pitting formation potential E_{pit} and protection potential E_p for pure aluminum are indicated by dashed line.

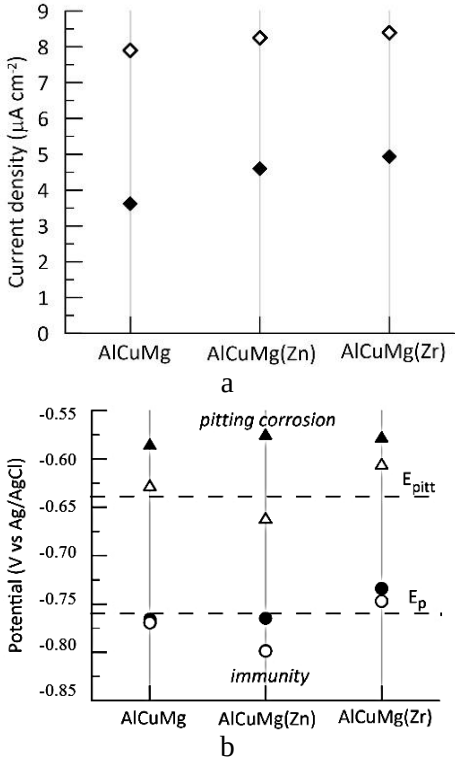

Fig. 5. Effect of the addition of Zn or Zr to amorphous (thick symbols) and nanocrystalline (hollow symbols) alloy AlCuMg on: (a) corrosion current density I_{corr}, and (b) pitting formation potential Potentials of pitting formation E_{pit} and protection E_p

Рис. 5. Влияние добавки Zn или Zr в аморфный (жирные символы) и нанокристаллический (полые символы) сплав AlCuMg на: (a) плотность тока коррозии I_{corr} и (b) потенциал образования питтинга Возможности питтингового образования E_{pit} и защиты E_p

The addition of 1 at.% Zn or 0.3 at.% Zr results in a slight increase of the corrosion current density without significantly affecting the value of E_{pit}. The potential E_{pit} for all three amorphous alloys remains more positive than that of the pure aluminum, which is indicative of a better resistance to pitting corrosion due to the amorphous state of the alloys. The protection potentials E_p for the base alloy $Al_{74}Cu_{16}Mg_{10}$ and for the Zn-containing amorphous alloys are identical and more negative than that of the aluminum standard. In this respect, it can be said that zirconium expands the immunity region of amorphous and nanocrystalline alloy $(Al_{74}Cu_{16}Mg_{10})_{99.7}Zr_{0.3}$. For this alloy E_p is the most positive and close to that of polycrystalline aluminum.

The formation of nanocrystalline structure due to annealing reduces the corrosion resistance of the alloys. The corrosion current density i_{corr} of nanocrystalline alloys increases almost twice compared to their amorphous analogues and the pitting formation potential E_{pit} shifts in negative direction. This shift is most visible in the nanocrystalline alloy $(Al_{74}Cu_{16}Mg_{10})_{99}Zn$-a, for which the largest negative shift of the protection potential E_p is registered.

The more positive values of OCP (Fig. 3) and E_{corr} (Fig. 5b) of the amorphous alloys $Al_{74}Cu_{16}Mg_{10}$, $(Al_{74}Cu_{16}Mg_{10})_{99}Zn$, and $(Al_{74}Cu_{16}Mg_{10})_{99.7}Zr_{0.3}$ compared to the potentials of their nanocrystalline counterparts and the respective lower corrosion current i_{corr} in them are most probably due to the denser passive film – layer of amorphous oxides formed on their surfaces. In this way better protection properties are ensured compared to the oxy-hydroxy films that are formed on the surfaces of their crystalline analogues.

DISCUSSION

The corrosion processes in amorphous alloys depend both on the corrosion environment and the chemical and structural inhomogeneities of the surface. It is known that in aqueous electrolytes a film composed of oxide and hydroxide layers forms on the surface of aluminum alloys [22]. The layer closest to the metal surface is amorphous with thickness depending on the composition and the temperature of the corrosive environment. The outer layers are relatively thicker and hydrated. During the corrosion process, the individual oxides and oxy-hydroxides are transformed into each other as a result of recrystallization and dehydration processes [20]. In case of continuous immersion, the protective alumina (Al_2O_3) turns into a white gel-like water soluble product $AlCl_3xH_2O$ [23] without protective properties. We observed its presence as "fluffy clouds" in the optical photographs of the amorphous alloy $(Al_{74}Cu_{16}Mg_{10})_{99}Zn$ after 200 h immersion in 3.5% NaCl (Fig. 6b).

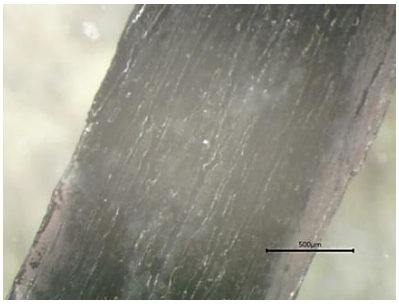

a

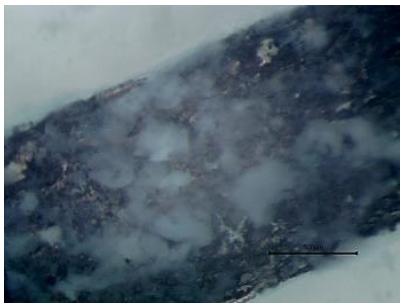

b

Fig. 6. In situ corrosion of amorphous alloy $(Al_{74}Cu_{16}Mg_{10})_{99}Zn$ in real time. a) After 24 h corrosion test; b) After 200 h corrosion test

Рис. 6. Коррозия на месте аморфного сплава $(Al_{74}Cu_{16}Mg_{10})_{99}Zn$ в реальном времени. a) После 24-ч испытания на коррозию; b) После 200-ч испытания на коррозию

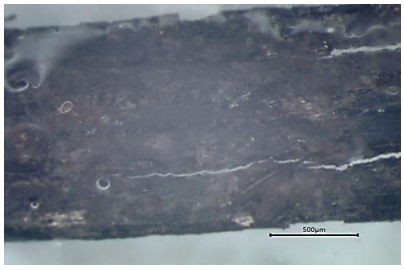

Fig. 7. Corrosion cleavage of alloy $(Al_{74}Cu_{16}Mg_{10})_{99}Zn$-a after 360 h in NaCl at 50 °C

Рис. 7. Коррозионное растрескивание сплава $(Al_{74}Cu_{16}Mg_{10})_{99}Zn$-a после 360 ч в NaCl при 50 °C

The microscopic observation of the surface of alloy $(Al_{74}Cu_{16}Mg_{10})_{99}Zn$ showed reddish areas probably enriched in Cu (Fig. 6a, b), which confirmed the presence of chemical inhomogeneity in the amorphous alloy. The areas enriched in Cu in the amorphous alloys and the $AlCu_2$ phase in the nanocrystalline samples (data from XRD analysis in Fig. 1 and Table 1) act as cathodes in respect to the anode alumina matrix and form micro galvanic elements, which are potential sites for development of local corrosion [24]. This process is particularly active in nanocrystalline samples tested at 50 °C. The high annealing temperature facilitates the diffusion and separation of copper at the grain boundaries and accelerates the course of local corrosion. As a result of these segregation processes, the continuous immersion in corrosive chloride medium leads to cor-

rosion cleavage of the samples. After a 360 h immersion in corrosive environment at 50 °C, the nanocrystalline samples $(Al_{74}Cu_{16}Mg_{10})_{99}Zn$ were broken into small pieces or entirely decomposed (Fig. 7).

The base alloy $Al_{74}Cu_{16}Mg_{10}$ in amorphous and nanocrystalline state has a lower corrosion rate at 25 °C than the Zn- or Zr-containing alloys since it contains only two phases, both with anode behavior – α-Al and Al_2CuMg [25, 26] (Table 1). Apart from the anode and cathode phases $Al_2(Cu, Zn)$ the amorphous and nanocrystalline Zn- and Zr- containing alloys [24] also contain Al_3Zr_4 (Table 1), which is a prerequisite for increasing the number and type of corrosive microgalvanic elements and accelerated galvanic corrosion. The electrochemically active intermetallic phases Al_2CuMg, $Al_2(Cu,Zn)$ and Al_3Zr_4 enhance the propensity to local corrosion and in particular to pitting corrosion [27].

The increased corrosion rates Kr_{50} of both Zr-containing amorphous alloy and Zn-containing nanocrystalline alloy at 50 °C are most likely due to the temperature instability of the formed non- amorphous multicomponent oxide surface layer [13, 28], which allows diffusion and contact of chloride ions with the metal surface.

It is found that zirconium and its alloys are sensitive to pitting corrosion in environments containing chloride ions [29], which is expressed in destruction of the tin passive film and subsequent localization of the corrosion process. There is insufficient evidence in the scientific literature on the mechanism of corrosion of Zr-amorphous alloys and the reasons for propensity of Zr-amorphous alloys to pitting corrosion have not yet been clarified. There is evidence that after testing of Zr-amorphous alloy in salt spray test of 5% NaCl solution, small amounts of tetragonal ZrO_2 crystals were found in the amorphous passive layer [13, 30]. Mudali et alt. [31] suggest that the existing physical imperfections (roughness, streaks, bulges /depressions) or chemical inhomogeneities on the surface of Zr-amorphous ribbons are attractive areas for adsorption of chloride ions and onset of pitting. Once the pitting has been initiated, their rapid uniform distribution on the surface of the amorphous band begins.

Our investigation confirmed that the corrosion characteristics of amorphous alloys depend on the type, size and distribution of surface nanoscale heterogeneities [26]. Asami et al. [32] prove that there is a critical size of the nano heterogeneities (about 20 nm) above which pitting is initiated. Local corrosion phenomena are also provoked by the activity of the galvanic pair - nanoscale heterogeneity / amorphous matrix. Interactions are possible between the pitting itself, caused by local chemical inhomogeneities, the density and distribution of nanophases.

CONCLUSIONS

At test temperature of 25 °C corrosion rate of amorphous alloys $Al_{74}Cu_{16}Mg_{10}$, $(Al_{74}Cu_{16}Mg_{10})_{99}Zn$ and $(Al_{74}Cu_{16}Mg_{10})_{99.7}Zr_{0.3}$ is respectively 4.0, 2.5 and 1.5 times lower than the corrosion rate of their crystalline analogues.

The lowest corrosion rate at 25 °C is measured for the base amorphous alloy $Al_{74}Cu_{16}Mg_{10}$.

At test temperature of 50 °C the corrosion rate of the amorphous alloy $(Al_{74}Cu_{16}Mg_{10})_{99.7}Zr_{0.3}$ is twice higher than the corrosion rate of the amorphous base alloy $Al_{74}Cu_{16}Mg_{10}$.

The corrosion rate of the nanocrystalline alloy $(Al_{74}Cu_{16}Mg_{10})_{99.7}Zr_{0.3}$-a is almost 3.5 times higher than the corrosion rate of the base nanocrystalline alloy $Al_{74}Cu_{16}Mg_{10}$-a.

The transformation of the amorphous into nanocrystalline structure accelerates the corrosion rate of all tested alloys at 25 °C.

The transformation of the amorphous into nanocrystalline structure accelerates dramatically the corrosion rate of $(Al_{74}Cu_{16}Mg_{10})_{99}Zn$ alloy at temperature of corrosion environment of 50 °C compared to the corrosion rate in the same environment at 25 °C.

The main reason for development of local corrosion in alloys $Al_{74}Cu_{16}Mg_{10}$, $(Al_{74}Cu_{16}Mg_{10})_{99}Zn_1$, and $(Al_{74}Cu_{16}Mg_{10})_{99.7}Zr_{0.3}$ are the chemical and surface structural inhomogeneities and the presence of active cathode electrochemical intermetallic phases Al_2CuMg, $Al_2(Cu,Zn)$, and Al_3Zr_4 in the anode aluminum matrix.

The research in this publication is funded under the project "Study of the rheological and corrosion behavior of amorphous and nanocrystalline aluminum-based alloys", Contract with BNCF № KP-06-H37 /13 from 06 December 2019.

The authors declare the absence a conflict of interest warranting disclosure in this article.

Исследование в данной публикации финансируется в рамках проекта «Исследование реологических и коррозионных свойств аморфных и нанокристаллических сплавов на основе алюминия», Контракт с BNCF № KP-06-H37/13 от 06.12.2019 г.

Авторы заявляют об отсутствии конфликта интересов, требующего раскрытия в данной статье.

REFERENCES
ЛИТЕРАТУРА

1. **Naka M., Hashimoto K., Masumoto T.** Corrosion resistivity of amorphous Fe alloys containing Cr. *Metals J. Jpn. Inst.* 1974. N 38 P. 835–8418.
2. **Souzaa A.C., Ribeiroa D.V., Kiminam C.S.** Corrosion resistance of Fe-Cr-based amorphous alloys: An overview. *J.*

Non-Crystall. Sol. 2016. V. 442. N 15. P. 56-66. DOI: 10.1016/j.jnoncrysol.2016.04.009.
3. **Pang S.J., Zhang T., Asami K., Inoue A.** Synthesis of Fe–Cr–Mo–C–B–P bulk metallic glasses with high corrosion resistance. *Acta Mater.* 2002. V. 50. N 3. P. 489–494. DOI: 10.1016/S1359-6454(01)00366-4.
4. **Bala H., Szymura S.** Acid corrosion of amorphous and crystalline Cu-Zr alloys. *Appl. Surf. Sci.* 1989. V. 35. N 1. P. 41-51. DOI: 10.1016/0169-4332(88)90036-0.
5. **Mudali U.K., Scudino S., Kühn U., Eckert J., Gebert A.** Polarisation behaviour of the $Zr_{57}Ti_8Nb_{2.5}Cu_{13.9}Ni_{11.1}Al_{7.5}$ alloy in different microstructural states in acid solutions. *Scripta Mater.* 2004. N 50. P. 1379–1384. DOI: 10.1016/j.scriptamat.2004.02.039.
6. **Akiyama E., Habazaki H., Kawashima A., Asami K., Hashimoto K.** Corrosion-resistant amorphous aluminum alloys and structure of passive films. *Mater. Sci. Eng.: A.* 1997. V. 226-228. P. 920-924. DOI: 10.1016/S0921-5093(96)10819-4.
7. **Aburada T., Unlu N., Fitz-Gerald J.M., Shiflet G.J., Scully J.R.** Effect of Ni as a minority alloying element on the corrosion behavior in Al–Cu–Mg–(Ni) metallic glasses. *Scripta Materialia*. 2008. V. 58. N 8. P. 623-626. DOI: 10.1016/j.scriptamat.2007.11.041.
8. **Mehmood M., Zhang B.P., Akiyama E., Habazaki H., Kawashima A., Asami K., Hashimoto K.** Experimental evidence for the critical size of heterogeneity areas for pitting corrosion of Cr-Zr alloys in 6 M HCl. *Corros. Sci.* 1998. V. 40. N 1. P. 1–17. DOI: 10.1016/S0010-938X(97)00107-8.
9. **Shanlin Wang**. Corrosion Resistance and Electrocatalytic Properties of Metallic Glasses. Metallic Glasses - Formation and Properties. *INTECH*. 2016. Chap. 4. P. 63-96. DOI: 10.5772/63677.
10. **Li W.H., Chana K.C., Xiaa L., Liuc L., He Y.Z.** Thermodynamic, corrosion and mechanical properties of Zr-based bulk metallic glasses in relation to heterogeneous structures. *Mater. Sci. Eng.: A.* 2012. V. 534. N 1. P. 157-162. DOI: 10.1016/j.msea.2011.11.054.
11. **Fehlner F.P., Frankenthal R.P., Kruger J.** Passivity of Metals. The Electrochemical Society. Pennington NJ. 1978.
12. **Fehlner F.P., Mott N.F.** Low-temperature oxidation. *Oxid Met.* 1970. N 2. 59 p.
13. **Ram Lim K., Park Jin Man., Soo Jee Sang., Kim S. Y., Kim S. J., Eun-Sung L., Kim W. T., Gebert A., Eckert J., Kim Do H.** Effect of thermal stability of the amorphous substrate on the amorphous oxide growth on Zr–Al–(Cu,Ni) metallic glass surfaces. *Corr. Sci.* 2013. N 73. P. 1-6. DOI: 10.1016/j.corsci.2013.04.009.
14. **Inoue Akihisa.** Amorphous, nanoquasicrystalline and nanocrystalline alloys in Al-based systems. *Prog. Mater. Sci.* 1998. N 43. P. 365-520. DOI: 10.1016/S0079-6425(98)00005-X.
15. **Effenberg G., Prince A.** Turnary Al-Cu-Mg diagram. *MSIT Workplace*. 2003. ID: 10.12587.2.20.
16. **Dyakova V., Stefanov G., Kovacheva D., Murdjeva Y.** Rapidly Solidified Al-Cu-Mg Amorphous and Nanocristalline Alloys. *Internat. J. "DNT Days"*. 2020. V. III. N 3. P. 154-159.
17. **Penkov I.G., Marinkov N.E., Stefanov G.N., Dyakova V.L., Kichukova D., Murdzjeva G.Y.S.** Glass forming ability and crystallization behaviour of amorphous and nanosized rapidly solidified $(Al_{75}Cu_{17}Mg_8)_{100-x}Zn_x$ alloys. *Int.. Sci. J. "Machines. Technologies. Materials"*. 2020. N 8. P. 366-369.
18. **Dyakova V., Stefanov G., Kovacheva D., Mourdjeva Y., Marinkov N., Penkov I., Georgiev J.** Influence of Zr and Zn as Minority Alloying Elements on Glass Forming Ability and Crystallization Behavior of Rapidly Solidified AlCuMg Ribbons. API Conf. TECHSYS Plovdiv Bulgaria- 2021. - in print.
19. **Dyakova V., Stefanov G., Penkov I., Kovacheva D., Marinkov N., Mourdjeva Y., Gyurov S.** Influence of Zn on glass forming ability and crystallization behaviour of rapidly solidified Al-Cu-Mg (Zn) alloys. *J. Chem. Technol. Metallurgy*. 2021. accepted for publication.
20. **Dyakova V., Kostova Y., Gyurov S., Kichukova D., Spasova H.** The influence of Zn on the corrosion behaviour of amorphous and nanosized rapidly solidified (Al75Cu17Mg8)100-xZnx alloys and their crystalline analogues. *Mater. Sci. Non-Equilibr. Phase Transform.* 2020. V. 6. N 3. P. 73-76.
21. **Dyakova V., Tzaneva B., Kostova Y.** Influence of Zn as Minority Alloying Element on the Uniform and Local Corrosion of Amorphous Rapidly Solidified AlCuMg(Zn) Ribbons. Proc. of 10th International Scientific Conference "Engineering, Technologies and Systems" (TechSys'2021). Plovdiv, Bulgaria. 27–29 May, 2021. AIP Conf. Proc. e-ISSN: 1551-7616.
22. **Harshmeet S.** The corrosion behaviour of aluminium alloy b206 in seawater. University of British Columbia. 2016.
23. **Orozco R., Genesca J., Juarez-Islas J.** Effect of Mg Content on the Performance of Al-Zn-Mg Sacrificial Anodes. *ASM Internat. JMEPEG*. 2007. N 16. P. 229–235. DOI: 10.1007/s11665-007-9037-z.
24. **Tao J.** Surface composition and corrosion behavior of an Al-Cu alloy. Chem. Phys. Université Pierre et Marie Curie - Paris V. English PA066159. 2016.
25. **Birbilis N., Cavanaugh M.K., Kovarik L., Buchheit R.G.** Nano-scale dissolution phenomena in Al–Cu–Mg alloys. *Electrochem. Commun.* 2008. N 10. P. 32–37. DOI: 10.1016/j.elecom.2007.10.032.
26. **Zhang S.D., Wang Z.M., Chang X.C., Hou W.L., Wang J.Q.** Identifying the role of nanoscale heterogeneities in pitting behaviour of Al-based metallic glass. *Corr. Sci*. 2011. V. 53. N 9. P. 3007-3015. DOI: 10.1016/j.corsci.2011.05.047.
27. **Birbilis N., Buchheit R.G.** Electrochemical characteristics of intermetallic phases in aluminum alloys an experimental survey and discussion. *J. Electrochem. Soc.* 2005. V. 152. N 4. P. B140-B151. DOI: 10.1149/1.1869984.
28. **McMahon M.E., Santucci R.J.Jr., Sculli J.R.** Advanced chemical stability diagrams to predict the formation of complex zinc compounds in a chloride environment. *RSC Adv*. 2019. N 9. P. 19905. DOI: 10.1039/C9RA00228F.
29. **Tsutsumi Y., Muto I., Nakano S., Tsukada J., Manaka T., Chen P., Ashida M., Sugawara Y., Shimojo M., Hara N., Katayama H., Hanawa T.** Effect of Impurity Elements on Localized Corrosion of Zirconium in Chloride Containing Environment. *J. Electrochem. Soc*. 2020. N 167. P. 141507. DOI: 10.1149/1945-7111/abc5d8.
30. **Zander D., Köster U.** Corrosion of amorphous and nanocrystalline Zr-based alloys. *Mater. Sci. Eng. A.* 2004. V. 375–377. P. 53–59. DOI: 10.1016/j.msea.2003.10.230.
31. **Mudaliab U.K., Baunacka S., Eckerta J., Schultza L., Geberta A.** Pitting corrosion of bulk glass-forming zirconium-based alloys. *J. Alloys Comp.* 2004. V. 377. N 1–2. P. 290-297. DOI: 10.1016/j.jallcom.2004.01.043.
32. **Zhanga B.P., Mehmoodb M., Habazakicand H., Hashimoto K.** Effects of nanoscale heterogeneity on thecorrosion behavior of non-equilibrium alloys. *Scripta Mater*. 2001. N 44. P. 1655–1658. DOI: 10.1016/S1359-6462(01)00879-X.

Поступила в редакцию (Received) 22.11.2021
Принята к опубликованию (Accepted) 28.02.2022